Design tool and guidelines for outdoor photobioreactors

Euntaek Lee, Jérémy Pruvost, Xing He, Ramakanth Munipalli, Laurent Pilon

Title
Design tool and guidelines for outdoor photobioreactors

Journal
Chemical Engineering Science, 106

ISSN
00092509

Authors
Lee, Euntaek
Pruvost, Jeremy
He, Xing
et al.

Publication Date
2014-03-01

DOI
10.1016/j.ces.2013.11.014

Peer reviewed

Design tool and guidelines for outdoor photobioreactors

Euntaek Lee[1], Jérémy Pruvost[2], Xing He[3],
Ramakanth Munipalli[3], and Laurent Pilon[1]

[1] Mechanical and Aerospace Engineering Department
Henry Samueli School of Engineering and Applied Science
University of California, Los Angeles - Los Angeles, CA 90095, USA
Phone: +1 (310)-206-5598, Fax: +1 (310)-206-2302
E-mail: pilon@seas.ucla.edu

[2] LUNAM Université, Université de Nantes, CNRS, GEPEA UMR 6144
Bd de lUniversité, CRTT-BP 406, 44602 Saint-Nazaire Cedex, France

[3] HyPerComp, Inc.
2629 Townsgate Rd., Suite 105, Westlake Village, CA, 91361, USA

E. Lee, J. Pruvost, X. He, R. Munipalli, and L. Pilon, 2014. "Design Tool and Guidelines for Outdoor Photobioreactors", *Chemical Engineering Science*, Vol. 106, pp. 18-29. doi:/10.1016/j.ces.2013.11.014

Abstract

This study provides design and operational guidelines for achieving maximum biomass productivity in outdoor photobioreactors (PBRs). Detailed simulations of coupled light transfer and growth kinetics of microalgae were performed for open ponds, vertical flat-plate, and tubular PBRs operated in batch mode and exposed to time-dependent collimated and diffuse solar irradiance. The temporal evolution of microalgae concentration was predicted by accounting for light saturation, photoinhibition, and respiration. Three-dimensional spectral light transfer simulations of collimated and diffuse solar radiation in the PBRs were performed at different times of the day. The green microalgae *Chlamydomonas reinhardtii* was used for illustration purposes. The study demonstrated that the daily productivity per unit of illuminated surface area for PBRs operated in batch mode was identical and depended uniquely on the ratio X_0/a where X_0 is the initial microalgae concentration and a is the illuminated surface area per unit volume of PBR. A maximum daily productivity of about 0.045 kg/m^2/day was achieved for X_0/a= 0.035 kg/m^2. Remarkably, similar results were obtained with experimental data and other simulation results based on different models reported in the literature, for different microorganisms and PBRs operated in continuous mode. The PBR optical thickness, represented by X_0/a, constitutes a convenient parameter for designing (via a) and operating (via X_0) these PBRs to achieve their maximum performance.

1 INTRODUCTION

Microalgae cultivation has received significant attention in recent years as a way to fixate CO_2 generated during fossil fuel combustion and to produce liquid or gaseous biofuels [1] as well as food supplement [2] and protein for human or animal feed [3]. Photosynthetic microalgae use sunlight as their energy source, water as their electron source, and CO_2 as their carbon source. They are typically grown in open ponds and photobioreactors (PBRs) of various designs where sunlight is absorbed and scattered by the microalgae kept in suspension by mechanical stirring and/or bubble sparging [4]. To be economically viable, the processes require the highest microalgae productivity and efficiency. Open ponds or PBRs can be operated in batch or in continuous mode. Batch cultures are widely used for their simplicity, flexibility, and low cost [5]. Scaling-up benchtop PBRs to industrial scale remains a challenge [6]. Indeed, optimum temperature, mixing, light, and mass transfer should be maintained in photobioreactors of any sizes [7]. Current photobioreactors must be improved in order to achieve larger mass concentrations and growth rate and to minimize auxiliary energy use and capital cost [8].

The objective of this study is to develop accurate numerical simulation tools and to obtain design guidelines for the optimization and operation of efficient PBRs. To do so, light transfer in PBRs with various geometries exposed to solar radiation was analyzed on a spectral basis over the spectral region between 400 and 700 nm corresponding to the photosynthetically active radiation (PAR) region. The temporal evolution of microalgae concentration was also predicted using growth kinetics model taking into account the local available light in the PBRs at different times of the day.

2 BACKGROUND

2.1 Radiation Transfer in Photobioreactors

As light travels through the microalgae suspension contained in the PBR, it is absorbed by the microorganisms or by the medium and scattered by microorganisms and, possibly, by gas bubbles used to deliver CO_2 and to stir the suspension. Solar radiation intensity $I_\lambda(\mathbf{r}, \hat{\mathbf{s}})$ at location $\mathbf{r}$ traveling along direction $\hat{\mathbf{s}}$ is governed by the radiative transfer equation (RTE) [1].

The local spectral fluence rate, denoted by $G_\lambda(\mathbf{r})$, and the local fluence rate average over the PAR region between 400 and 700 nm, denoted by $G_{PAR}(\mathbf{r})$, available to microalgae at location $\mathbf{r}$ are respectively defined as [1],

$$G_\lambda(\mathbf{r}) = \int_{4\pi} I_\lambda(\mathbf{r}, \hat{\mathbf{s}}) \mathrm{d}\Omega \quad \text{and} \quad G_{PAR}(\mathbf{r}) = \int_{400}^{700} G_\lambda(\mathbf{r}) \mathrm{d}\lambda \tag{1}$$

The average fluence rate G_{av} over the entire PBR of volume V can be estimated from the local PAR-averaged fluence rate $G_{PAR}(\mathbf{r})$ as,

$$G_{av} = \frac{1}{V} \int_V G_{PAR}(\mathbf{r})\, dV = \frac{1}{V} \int_V \left(\int_{400}^{700} G_\lambda(\mathbf{r})\, d\lambda \right) dV \tag{2}$$

The two-flux approximation assumes one-dimensional radiation transfer and can account for in-scattering terms as well as anisotropic scattering [18] and provides a simple analytical expression for the local spectral fluence rate $G_\lambda(z)$ [10,15]. In cases when the PBR is exposed to both collimated and diffuse irradiances $G_{in,c,\lambda}$ and $G_{in,d,\lambda}$, the total local spectral fluence rate $G_\lambda(z)$ (in W/m^2) can be estimated by summing up its collimated and diffuse components as [28],

$$G_\lambda(z) = G_{c,\lambda}(z) + G_{d,\lambda}(z) \tag{3}$$

Pottier *et al.* [11] solved the radiative transfer equation (RTE) using the two-flux approximation to model light transfer in a one-dimensional flat-plate photobioreactor with a transparent front window and a diffusely reflecting back side with spectral reflectance ρ_λ. The authors derived an analytical expression for the local spectral fluence rate $G_{c,\lambda}(z)$ (in W/m^2) in such PBRs exposed to solar irradiance $G_{in,c,\lambda}$ incident onto the photobioreactor at an angle θ_c with respect to the surface's normal direction as [11],

$$\frac{G_{c,\lambda}(z)}{G_{in,c,\lambda}} = 2\sec\theta_c \frac{[\rho_\lambda(1+\alpha_\lambda)e^{-\delta_\lambda L} - (1-\alpha_\lambda)e^{-\delta_\lambda L}]e^{\delta_\lambda z} + [(1+\alpha_\lambda)e^{\delta_\lambda L} - \rho_\lambda(1-\alpha_\lambda)e^{\delta_\lambda L}]e^{-\delta_\lambda z}}{(1+\alpha_\lambda)^2 e^{\delta_\lambda L} - (1-\alpha_\lambda)^2 e^{-\delta_\lambda L} - \rho_\lambda(1-\alpha_\lambda^2)e^{\delta_\lambda L} + \rho_\lambda(1-\alpha_\lambda^2)e^{-\delta_\lambda L}} \tag{4}$$

where the parameters α_λ and δ_λ are expressed as [11],

$$\alpha_\lambda = \sqrt{\frac{\bar{A}_{abs,\lambda}}{\bar{A}_{abs,\lambda} + 2b_\lambda \bar{S}_{sca,\lambda}}} \quad \text{and} \quad \delta_\lambda = X\sec\theta_c \sqrt{\bar{A}_{abs,\lambda}(\bar{A}_{abs,\lambda} + 2b_\lambda \bar{S}_{sca,\lambda})} \tag{5}$$

here $\bar{A}_{abs,\lambda}$ and $\bar{S}_{sca,\lambda}$ are the average mass absorption and scattering cross-sections (in m^2/kg) while X is the microorganism mass concentration X expressed in kg dry cell weight cells per m^3 of suspension (or kg/m^3). The effective absorption and scattering coefficients of the suspension are given by

$$\kappa_\lambda = \bar{A}_{abs,\lambda} X \quad \text{and} \quad \sigma_{s,\lambda} = \bar{S}_{sca,\lambda} X \tag{6}$$

For an axisymmetric phase function, the backward scattering fraction, denoted by b_λ is defined as [11],

$$b_\lambda = \int_{\pi/2}^{\pi} \Phi_{T,\lambda}(\theta)\sin\theta \mathrm{d}\theta \tag{7}$$

where $\Phi_{T,\lambda}(\hat{\mathbf{s}}_i, \hat{\mathbf{s}})$ is the effective scattering phase function of the suspension. The local diffuse spectral fluence rate $G_{d,\lambda}(z)$ can be estimated from Eqs. 4 and 5 by replacing by a factor 2.

2.2 Microalgae Growth Kinetics

The time rate of change of microalgae mass concentration X can be modeled as [38],

$$\frac{dX}{dt} = \bar{\mu} X \tag{8}$$

where $\bar{\mu}$ is the average total specific growth rate expressed in hr^{-1}. Various growth kinetics models have been developed to predict the local specific growth rate μ. Fouchard *et al.* [21]

expressed the photosynthetic growth rate of *C. reinhardtii* as a function of local fluence rate $G_{PAR}(\mathbf{r})$ at location $\mathbf{r}$, according to the Haldane model [39], accounting for light limitation and inhibition as

$$\mu_p(\mathbf{r}) = \mu_0 \left(\frac{G_{PAR}(\mathbf{r})}{K_S + G_{PAR}(\mathbf{r}) + G^2_{PAR}(\mathbf{r})/K_I} \right) \tag{9}$$

where μ_0 is the so-called maximum specific growth rate while the coefficients K_S and K_I are the light half-saturation and inhibition constants, respectively. The authors also considered reduction in growth rate due to cellular respiration as the catabolic process. Then, the total local specific grow rate $\mu(\mathbf{r})$ can be expressed as [21]

$$\mu(\mathbf{r}) = \mu_p(\mathbf{r}) - \mu_s \tag{10}$$

where μ_s is the respiration rate and was assumed to be constant at all times and locations [21]. In addition, the average total specific growth rate $\bar{\mu}$ over the PBR volume can be estimated as [21]

$$\bar{\mu} = \frac{1}{V} \int_V \mu(\mathbf{r}) dV \tag{11}$$

2.3 Photobioreactor Modeling

Modeling of PBR typically consists of solving the RTE coupled with a growth kinetics model. Aiba [9] calculated the light intensity distribution and absorptance in one-dimensional flat-plate photobioreactor with microalgae *Rhodopseudomonas spheroides* using the Monte Carlo method. The author considered anisotropic scattering and neglected reflection at the walls. He compared the absorptance obtained by the Monte Carlo method with that obtained by Beer-Lambert's law as a function of cell concentration. Beer-Lambert's law was found to overestimate the absorptance in the photobioreactor because it does not consider in-scattering [9]. This was also illuestablished in Ref. [19].

Cornet *et al.* [10], Cornet and Albiol [20], and Cornet and Dussap [12] developed a coupled light transfer and Haldane growth kinetics model to estimate the biomass volumetric production rate of one-dimensional flat-plate PBRs. They introduced the concept of working illuminated volume which, combined with their models, can be used to retrieve the growth kinetic parameters. Based on this approach Fouchard *et al.* [21] retrieved the growth kinetics parameters of *C. reinhardtii* cultivated in a torus PBR with continuous injection of N_2 and CO_2 gases and illuminated with white light from fluorescent tubes considering biomass concentration, extracellular sulfur concentration, and intracellular quota. Finally, these models have been validated experimentally for different (i) PBR shapes and volumes, (ii) incident irradiance, (iii) microorganism species, and (iv) carbon sources.

Wheaton and Krishnamoorthy [22] simulated light transfer coupled with fluid hydrodynamics within an air-lift tubular photobioreactor illuminated from inside by fluorescent lamps. The authors identified the effects of angular discretization, scattering phase function, air mass flow rate, and bubble size on the local fluence rate. They used finite volume method to solve the 3D RTE based on spectrally averaged incident radiation and radiation characteristics of cyanobacterium *Synechococcus sp.* over three spectral bands in the PAR

region. They concluded that scattering by bubbles resulted in redistribution of the light but was negligible at high microalgae concentrations, as previously reported [23].

Murphy and Berberoğlu [24] coupled light transfer with photosynthetic rate model for *C. reinhardtii* wild strain and transformant *tla1* within plane parallel PBR considering photoinhibition. The authors solved the one-dimensional RTE using the discrete ordinates method with Gaussian quadrature to estimate the local fluence rate. They calculated the local specific and total oxygen production as function of optical thickness for different incident irradiances.

Slegers *et al.* [13] simulated outdoor vertical flat-plate PBRs operated in continuous mode and containing *Phaeodactylum tricornutum* or *Thalassiosira pseudonana*. The authors coupled light transfer with a growth kinetics model to estimate volumetric daily and yearly biomass productivity. They treated the suspensions as gray with constant radiation characteristics averaged over the PAR region and used Beer-Lambert's law to calculate the average fluence rate within the PBR and a growth kinetic model based on pI-curves and accounting for respiration [25]. They also defined the average total specific growth rate based on Equation (11). They investigated the effect of thickness of PBRs and biomass concentration on the volumetric productivity in the Netherlands.

Huang *et al.* [26] simulated annular PBR with *Porphyridium cruentum* in continuous and batch cultures. The authors integrated hydrodynamics, radiation transfer, and growth kinetics models to predict biomass concentration as a function of time. The 3D RTE was solved using finite volume method and discrete ordinate method to estimate the light intensity within the annular PBR. The box model with two boxes was used to account for spectral radiation in normal diffuse incident irradiance and radiation characteristics of microalgae to estimate the light intensity within the annular PBR. Good agreement was observed between the numerically prediction of biomass concentration and experimental data reported in the literature [27].

Finally, Pruvost *et al.* [28] simulated outdoor inclined rectangular PBR exposed to solar irradiance with cyanobacterium *Arthrospira platensis* grown in continuous culture. The authors coupled light transfer with growth kinetics model to estimate the areal biomass productivity per unit surface area illuminated. They calculated the fluence rate using the two-flux approximation [15] for constant biomass concentration. They investigated the effects of latitude and inclination of the PBR surface on the maximum areal biomass productivity. The location close to the earth equator had biomass productivity up to 40% larger than those at higher latitudes. In addition, the areal biomass productivity achieved with a solar tracking system was 30% larger than that obtained with constant inclination.

Previous studies often used spectrally averaged incident irradiance and radiation characteristics [9, 10]. In addition, light transfer in PBRs has frequently been treated as one-dimensional [10–12] and estimated using either Beer-Lambert's law [13] or the two-flux approximation [10, 14, 15]. Most studies also considered constant and normally collimated incident irradiance [11,12,16]. However, solar irradiance fluctuates in direction and intensity during the day. Also, radiation characteristics of microalgae depends strongly on wavelength. In addition, actual PBRs may have complex geometries for which simplified radiation model may not be valid.

Moreover, [53], [54] and [55] suggested the need for a unifying approach to PBR design and operation and emphasized the connection between light intensity, cell density, and the

optical thickness of the PBR to maximize microalgal productivity. The authors demonstrated the need to optimize these parameters for a given microalgae species and provided qualitative guidelines obtained from experimental studies. In particular, they recommended ultra-high cell density cultures in PBRs with short path length to achieve efficient utilization of solar radiation. Under these conditions, they also discussed the importance of turbulent mixing to increase the light/dark cycle frequency. However, quantitative criteria for optimum productivity were not provided.

In this study, light transfer was accurately simulated by solving the three-dimensional RTE on a spectral basis using experimentally measured spectral radiation characteristics [17]. Both spectral diffuse and collimated solar irradiances with different incident angle corresponding to different times of the day were considered. It was coupled with the Haldane growth kinetics model accounting for photolimitation, photoinhibition, and cellular respiration. The fluence rate, biomass concentration, and daily productivity of open ponds, vertical flat-plate, and tubular PBRs were compared and discussed with experimental and numerical results reported in the literature. Quantitative criteria to achieve maximum productivity were also derived in terms of cell density and PBR dimensions for a given microalgae species.

3 METHODS

3.1 Problem Statement

Algal biomass production in PBRs depends on numerous parameters including (i) the cultivation location, (ii) the day of the year and the time of the day along with (iii) the corresponding solar irradiance, (iv) the microalgae species, (v) the initial mass concentration, (vi) the PBR geometry, and (vii) its wall reflection and refraction. The present study simulates light transfer and microalgae growth in common PBRs located in Los Angeles, CA USA (34.04°N, 118.15°W). Simulations were performed for open pond, vertical flat-plate, and tubular PBRs. The PBRs were aligned along the north-south direction and exposed to solar irradiance comprised of both a collimated and a diffuse component. Figure 1 shows the geometries, dimensions, and boundary conditions of the PBRs simulated in this study along with the associated coordinate systems. The open pond had depth L varying from 0.05 to 1.0 m. The thickness L of the vertical flat-plate PBR ranged from 0.05 to 1.0 m while the diameter L of the tubular PBR varied from 0.1 to 1.0 m. *C. reinhardtii* were simulated for illustration purposes and because its growth kinetic parameters were known [21].

3.2 Assumptions

In order to predict light transfer and the temporal evolution of microalgae concentration in the different PBRs considered, it was assumed that: (1) the microalgae were well mixed, randomly oriented, and uniformly distributed in the PBR. In practice, this is achieved by stirring the PBR with paddle wheels or gas sparging, for example. (2) The liquid medium was non-emitting (cold) and non-scattering over the PAR region. (3) The absorption coefficient of the medium was the same as that of water. (4) The radiation characteristics of *C. reinhardtii* remained the same throughout the day. (5) Bubbles potentially used for stirring purposes

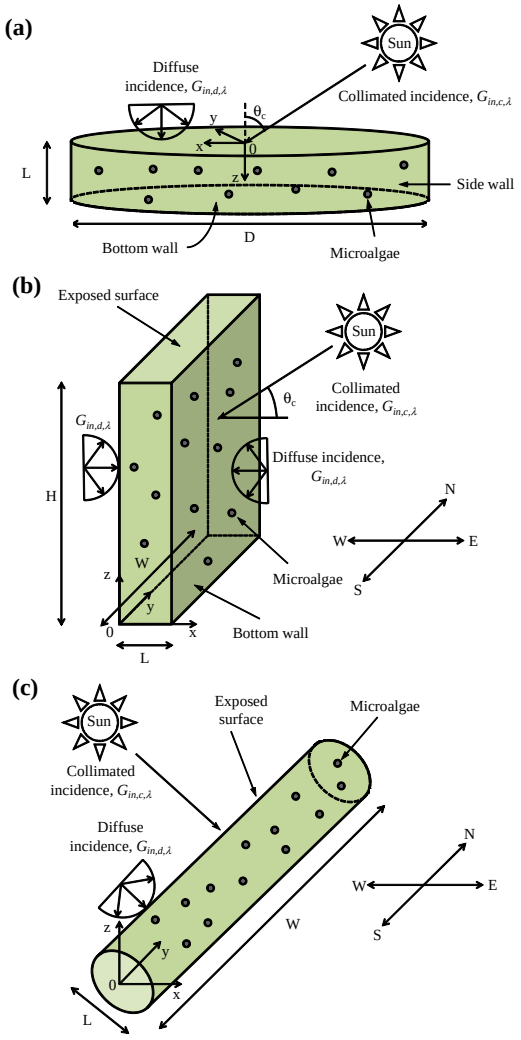

Figure 1: Schematic of the (a) open pond, (b) vertical flat-plate, and (c) tubular photobioreactors simulated in this study along with coordinate systems.

featured interfacial area concentration smaller than 450 m^{-1} so their effect on light transfer could be neglected [23]. (6) The PBR was neither mass transfer nor nutrient limited and operated at constant temperature. (7) The photosynthetic specific growth rate μ_p was only a function of the local and average fluence rate available in the PBRs and given by Equations (9), and (8) Finally, biomass loss at night due to respiration was ignored as PBR productivity was estimated after 12 h of exposure to sunlight. For longer duration (succession of day-night cycles), losses to the respiration at night must be considered [56]

3.3 Governing Equations

The radiation intensity $I_\lambda(\mathbf{r}, \hat{\mathbf{s}})$ in direction $\hat{\mathbf{s}}$ at location $\mathbf{r}$ can be decomposed as the sum of a collimated $I_{c,\lambda}(\mathbf{r}, \hat{\mathbf{s}})$ and a diffuse $I_{d,\lambda}(\mathbf{r}, \hat{\mathbf{s}})$ component so that [18],

$$I_\lambda(\mathbf{r}, \hat{\mathbf{s}}) = I_{c,\lambda}(\mathbf{r}, \hat{\mathbf{s}}) + I_{d,\lambda}(\mathbf{r}, \hat{\mathbf{s}}) \tag{12}$$

The steady-state RTE for the collimated intensity can be written as [18],

$$\hat{\mathbf{s}} \cdot \nabla I_{c,\lambda}(\mathbf{r}, \hat{\mathbf{s}}) = -\kappa_\lambda I_{c,\lambda}(\mathbf{r}, \hat{\mathbf{s}}) - \sigma_{s,\lambda} I_{c,\lambda}(\mathbf{r}, \hat{\mathbf{s}}) \tag{13}$$

This first and second terms on the right-hand-side of Eq. 13 account for the fact that the collimated incident radiation along the collimated direction decays as it travels through the microalgae suspension due to absorption and scattering, respectively. Similarly, the steady-state RTE for the diffuse intensity $I_{d,\lambda}(\hat{r}, \hat{s})$ can be written as [18],

$$\begin{aligned} \hat{\mathbf{s}} \cdot \nabla I_{d,\lambda}(\mathbf{r}, \hat{\mathbf{s}}) &= -\kappa_\lambda I_{d,\lambda}(\mathbf{r}, \hat{\mathbf{s}}) - \sigma_{s,\lambda} I_{d,\lambda}(\mathbf{r}, \hat{\mathbf{s}}) + \frac{\sigma_{s,\lambda}}{4\pi} \int_{4\pi} I_{d,\lambda}(\mathbf{r}, \hat{\mathbf{s}}_i) \Phi_\lambda(\hat{\mathbf{s}}_i, \hat{\mathbf{s}}) \mathrm{d}\Omega_i \\ &+ \frac{\sigma_{s,\lambda}}{4\pi} \int_{4\pi} I_{c,\lambda}(\mathbf{r}, \hat{\mathbf{s}}_i) \Phi_\lambda(\hat{\mathbf{s}}_i, \hat{\mathbf{s}}) \mathrm{d}\Omega_i \end{aligned} \tag{14}$$

The last two terms of Eq. 14 account for multiple scattering of the diffuse and collimated radiation intensities. In fact, the diffuse incident radiation along direction $\hat{\mathbf{s}}_i$ at location $\mathbf{r}$ is not only absorbed and scattered but also reinforced as diffuse and collimated radiations from any direction $\hat{\mathbf{s}}_i$ over 4π solid angle get scattered in direction $\hat{\mathbf{s}}_i$.

3.4 Radiation Characteristics of *C. reinhardtii*

The effective absorption coefficient κ_λ of the suspension can be expressed in terms of the microorganism mass concentration X as [40],

$$\kappa_\lambda = \kappa_{L,\lambda}(1 - \nu X) + \bar{A}_{abs,\lambda} X \tag{15}$$

where ν is the specific volume of microorganisms assumed to be equal to 0.001 m^3/kg. The absorption coefficient of the liquid phase $\kappa_{L,\lambda}$ is expressed in m^{-1} and given by [18],

$$\kappa_{L,\lambda} = \frac{4\pi k_\lambda}{\lambda} \tag{16}$$

where k_λ was taken as the absorption index of water reported by Hale and Querry [41]. On the other hand, the effective scattering coefficient $\sigma_{s,\lambda}$ of the suspension can be expressed as [42],

$$\sigma_{s,\lambda} = \bar{S}_{sca,\lambda} X \tag{17}$$

The average mass absorption and scattering cross-sections $\bar{A}_{abs,\lambda}$ and $\bar{S}_{sca,\lambda}$ along with the Henyey-Greenstein asymmetry factor of *C. reinhardtii* between 400 and 750 nm were reported in the literature [17]. Alternatively, they could have been predicted by Lorenz-Mie theory using the complex index of refraction retrieved by Lee *et al.* [43].

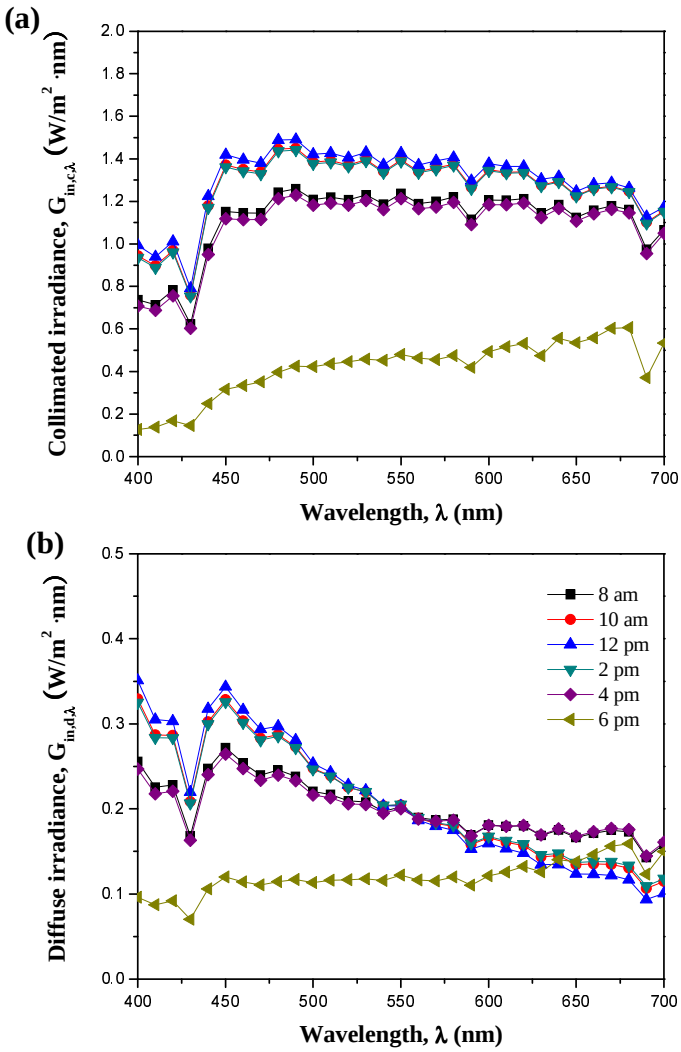

Figure 2: (a) collimated $G_{in,c,\lambda}$ and (b) diffuse $G_{in,d,\lambda}$ solar irradiance spectrum over the PAR region at 12:00 pm.

3.5 Boundary and Initial Conditions

The solar spectrum incident on Earth depends on the latitude, longitude, and altitude. In this study, the Simple Model of the Atmospheric Radiative Transfer of Sunshine (SMARTS) [44] was used to predict the incident collimated and diffuse solar irradiances at sea level in Los Angeles, CA on June 21 at different times of the day. Figure 2 shows the incident (a) collimated and (b) diffuse solar irradiances, denoted by $G_{in,c,\lambda}$ and $G_{in,d,\lambda}$, in the PAR region for different times of the day. These irradiances were used in the boundary conditions necessary to solve Equations (13) and (14) according to $I_{c,\lambda}(\mathbf{r}_{wall}, \hat{\mathbf{s}}) = G_{in,c,\lambda}$ and $I_{d,\lambda}(\mathbf{r}_{wall}, \hat{\mathbf{s}}) = G_{in,d,\lambda}/2\pi$, respectively. Here, the denominator 2π corresponds to the solid angle of the hemisphere through which the diffuse irradiance $G_{in,d,\lambda}$ is incident on the PBR [18].

The other boundary conditions depend on the PBR geometry. The open ponds were

assumed to have transparent top surface, i.e., reflection by air-water interface was neglected since it does not exceed 6% over the PAR region for incident angle within 60° of the normal to the pond surface according to Fresnels law [18]. Note that the pond surface is strongly reflecting at glazing incident angles corresponding to sunrise and sunset. Then, however, the intensity incident on the PBR was insufficient to significantly affect the biomass concentration. In addition, the bottom and side walls of the pond were treated as black ($\rho_\lambda = 0$) or diffusely reflecting ($\rho_\lambda = 1$). Refraction by the panels of the vertical flat-plate PBRs with constant index of refraction of 1.49 over the PAR region was also considered. The results were compared with those of simulations treating PBR walls as transparent. Based on result from the flat-plate PBRs, the wall of the tubular PBRs was assumed to be transparent and refraction by the tube wall was ignored, as discussed in Sections 4.2 and 4.3.

3.6 Two-Flux Approximation

The analytical expression derived by Cornet *et al.* [10] for predicting the local fluence rate G_λ(z) in vertical flat-plate PBRs exposed to collimated solar irradiance with reflecting back wall [Equation (4)] can be extended to vertical flat-plate PBRs with transparent faces, one exposed to direct collimated and diffuse incident solar irradiance $G_{in,c,\lambda}$ and $G_{in,d,\lambda}$ and the other exposed only to diffuse solar irradiance $G_{in,d,\lambda}$. Then, the local spectral fluence rate at time t can be expressed as

$$G_\lambda(z,t) = G_{in,c,\lambda}(t) f_c(z) + G_{in,d,\lambda}(t) f_d(z) + G_{in,d,\lambda}(t) f_d(L-z) \tag{18}$$

where $f_c(z)$ is defined as

$$f_c(z) = 2\sec\theta_c(t) \frac{(1+\alpha_\lambda)e^{\delta_\lambda L}e^{-\delta_\lambda z} - (1-\alpha_\lambda)e^{-\delta_\lambda L}e^{\delta_\lambda z}}{(1+\alpha_\lambda)^2 e^{\delta_\lambda L} - (1-\alpha_\lambda)^2 e^{-\delta_\lambda L}} \tag{19}$$

and $f_d(z)$ is expressed as

$$f_d(z) = 4\frac{(1+\alpha_\lambda)e^{\delta_{d,\lambda} L}e^{-\delta_{d,\lambda} z} - (1-\alpha_\lambda)e^{-\delta_{d,\lambda} L}e^{\delta_{d,\lambda} z}}{(1+\alpha_\lambda)^2 e^{\delta_{d,\lambda} L} - (1-\alpha_\lambda)^2 e^{-\delta_{d,\lambda} L}} \tag{20}$$

hereα_λ and δ_λ are given by Equation (5) while $\delta_{d,\lambda} = 2X\sqrt{\bar{A}_{abs,\lambda}(\bar{A}_{abs,\lambda} + 2b_\lambda \bar{S}_{sca,\lambda})}$.

Moreover, Berberoğlu *et al.* [17] reported that the Henyey-Greenstein asymmetry factor of *C. reinhardtii* was 0.98 corresponding to strongly forward scattering, typical of microalgae. Then, the backward scattering fraction b_λ given by Equation (7) can be assumed to be zero and $\alpha_\lambda \simeq 1$. Then, the fluence rate in vertical flat-plate PBR exposed to collimated and diffuse incident radiation simplifies to

$$G_\lambda(z,t) = \sec\theta_c(t) G_{in,c,\lambda}(t) e^{-\delta_\lambda z} + 2G_{in,d,\lambda}(t)\left[e^{-\delta_{d,\lambda} z} + e^{-\delta_{d,\lambda}(L-z)}\right] \tag{21}$$

where δ_λ and $\delta_{d,\lambda}$ simplify to $\delta_\lambda = \bar{A}_{abs,\lambda} X(t) \sec\theta_c(t)$ and $\delta_{d,\lambda} = 2\bar{A}_{abs,\lambda} X(t)$. Similarly, the fluence rate in open ponds with reflecting back wall can be expressed as

$$G_\lambda(z,t) = G_{in,c,\lambda}(t) f_c(z) + G_{in,d,\lambda}(t) f_d(z) \tag{22}$$

If $\alpha_\lambda \approx 1$, the two-flux approximation for open-ponds simplifies to

$$G_\lambda(z,t) = \left[G_{in,c,\lambda}(t)\sec\theta_c(t) + 2G_{in,d,\lambda}(t)\right]\left[e^{-\delta_\lambda z} + \rho_\lambda e^{-\delta_\lambda(2L-z)}\right] \tag{23}$$

These expressions apply also in the case of open ponds with black walls with $\rho_\lambda = 0$.

3.7 Method of solution

3.7.1 Light transfer

The 3D RTE given by Equations (13) and (14) were solved numerically for $I_\lambda(\mathbf{r}, \hat{\mathbf{s}})$ using the discontinuous Galerkin method. Detailed description of the DG method used in the present study and its validation was given in Ref. [35] and need not be repeated. Sunlight incident on the PBRs consists of a collimated and a diffuse component. The direction $\theta_c(t)$ of collimated incidence changed during the course of the day. Unfortunately, conventional angular discretization methods such as discrete ordinate S_N [45] and T_N [46] approximations typically use fixed discrete directions. Therefore, the discretization would need to be changed for simulating different hours of the day [47]. Discrete ordinate scheme with infinitely small weight (DOS+ISW) [47] was employed in this study to simulate collimated sunlight incident on the PBRs during the course of the day. It consists of adding a discrete direction, corresponding to the direction of collimated irradiance, directly to a conventional discrete ordinate quadrature. The weight associated with this new discrete direction is set to be infinitely small [47]. Thus, the new discrete direction has no effect on the zeroth, first, and second order moments of the intensity [47].

Finally, unstructured tetrahedral elements were employed for spatial discretization. The number of elements varied depending on the size of the PBRs. The maximum number of elements in simulating open ponds, vertical flat-plate, and tubular photobioreactors was 95633, 91257, and 112464, respectively. The S_4 angular discretization, consisting of 6 discrete ordinate directions per quadrant, was used. The PAR region, defined from 400 to 700 nm, was discretized in 10 nm increments for a total of 31 wavelengths. To obtain a numerically converged solution of the RTE, the P-3 DG method was used in all simulations. with a maximum number of elements in simulating open ponds, vertical flat-plate, and tubular PBRs equal to 95,633, 91,257, and 112,464, respectively.

3.7.2 Growth kinetics

In the present study, the growth kinetics model described by Equations (8) to (11) was used to determine the temporal evolution of microalgae concentration in photobioreactors. Fouchard *et al.* [21] measured the average specific growth rate $\bar{\mu}$ of the green algae *C. reinhardtii*. The authors estimated the parameters μ_0, μ_s, K_S, and K_I to be 0.2274 hr^{-1}, 0.032 hr^{-1}, 81.38 μmol photon $\text{m}^{-2}\cdot\ \text{s}^{-1}$, and 2500 μmol photon $\text{m}^{-2}\cdot\ \text{s}^{-1}$, respectively for local irradiance $G_{PAR}(\mathbf{r})$ ranging from 0 to 400 μmol photon $\text{m}^{-2}\cdot\ \text{s}^{-1}$. These parameters resulted in prediction for μ in good agreement with experimental data reported by [48]. They were used in the present study after converting K_S and K_I, expressed in μmol photon $\text{m}^{-2}\cdot\ \text{s}^{-1}$, in W/m^2 using the conversion factor, 1 μmol photon $\text{m}^{-2}\cdot\ \text{s}^{-1} \simeq 0.2174\ \text{W/m}^2$ over the PAR region [49].

3.7.3 Solution procedure

The mass concentration of microalgae as a function of time was obtained by the following procedure. First, the initial mass concentration of microalgae was set as $X(t = 0) = X_0$ at initial time 8:00 am. The corresponding effective absorption coefficient κ_λ and the scattering

coefficient $\sigma_{s,\lambda}$ were estimated using Equations (15) and (17), respectively. Then, Equations (13) and (14) were solved for $I_{\lambda,c}$ and for $I_{\lambda,d}$ using the DG method. Then, the local fluence rate was estimated using Equation (1). The corresponding local photosynthetic specific growth rate μ_p was estimated [Equation (9)] and used to calculate the average total specific growth rate $\bar{\mu}$ [Equation (11)] and the microalgae mass concentration $X(t)$ [Equation (8)] at subsequent time. This procedure was repeated by increment of 2 hours. During that time interval, the local fluence rate and average total specific growth rate were assumed to be constant. To assess the validity of this assumption, the temporal evolution of the concentration in open ponds was predicted for 12 hours with initial mass concentration X_0 = 0.1 kg/m^3 using the two-flux approximation and the same growth kinetics model. The local fluence rates obtained for time intervals of 30 minutes, 1 hours, and 2 hours were compared at 8:00 am, 10:00 am, 12:00 pm (noon), 2:00 pm, 4:00 pm, 6:00 pm, and 8:00 pm. The maximum relative errors in the corresponding $\bar{\mu}(t)$ and $X(t)$ throughout the day were less than 3% and 6%, respectively. Thus, a 2 hours time increment was judged appropriate for simulating coupled radiation transfer and microalgae growth kinetics in the PBR throughout the day.

4 RESULTS AND DISCUSSION

4.1 Open ponds

Figure 3 shows the local PAR-averaged fluence rate $G_{PAR}(\mathbf{r})$ in the east/west center plane of the open pond with either (a) black or (b) reflecting side and bottom walls at times 8:00 am, 10:00 am, 12:00 pm (noon), 2:00 pm, and 4:00 pm. Here, the pond diameter D, depth L, and initial mass concentration X_0 were taken as 2 m, 0.1 m, and 0.1 kg/m^3, respectively. By comparing Figures 3a and b, it is evident that the reflecting walls increased the local fluence rate in the PBR, particularly before 4:00 pm. However, the relative difference, in terms of mass concentration $X(t)$, between open ponds with black and reflecting walls was less than 1% after a day of growth. In both cases, the local fluence rate was nearly one-dimensional except near the side walls where shadows were apparent in the early morning and late afternoon. Note that even though, on June 21 in Los Angeles, the sun rises at 05:42 am and sets at 8:08 pm, the average total specific growth rate $\bar{\mu}$ at times earlier than 8:00 am and later than 8:00 pm was less than 0.01 hr^{-1} and growth was negligible.

4.2 Vertical flat-plate photobioreactor

Light transfer in a vertical flat-plate photobioreactor oriented north-south with initial mass concentration X_0 = 0.1 kg/m^3 was simulated over 12 hours. The vertical flat-plate PBR height H, width W, and thickness L were taken as 2 m, 2 m, and 0.1 m, respectively. The walls were made of 8 mm thick glass panels. The effect of refraction due to mismatch in refractive indices of the air (n = 1.0), the reactor walls (n = 1.49), and the *C. reinhardtii* suspension (n = 1.33) contained in the PBR was investigated. These refraction indices were assumed to be constant over the PAR region. Reflection and refraction were estimated using Fresnel's equations for optically smooth and specularly reflecting surfaces [18].

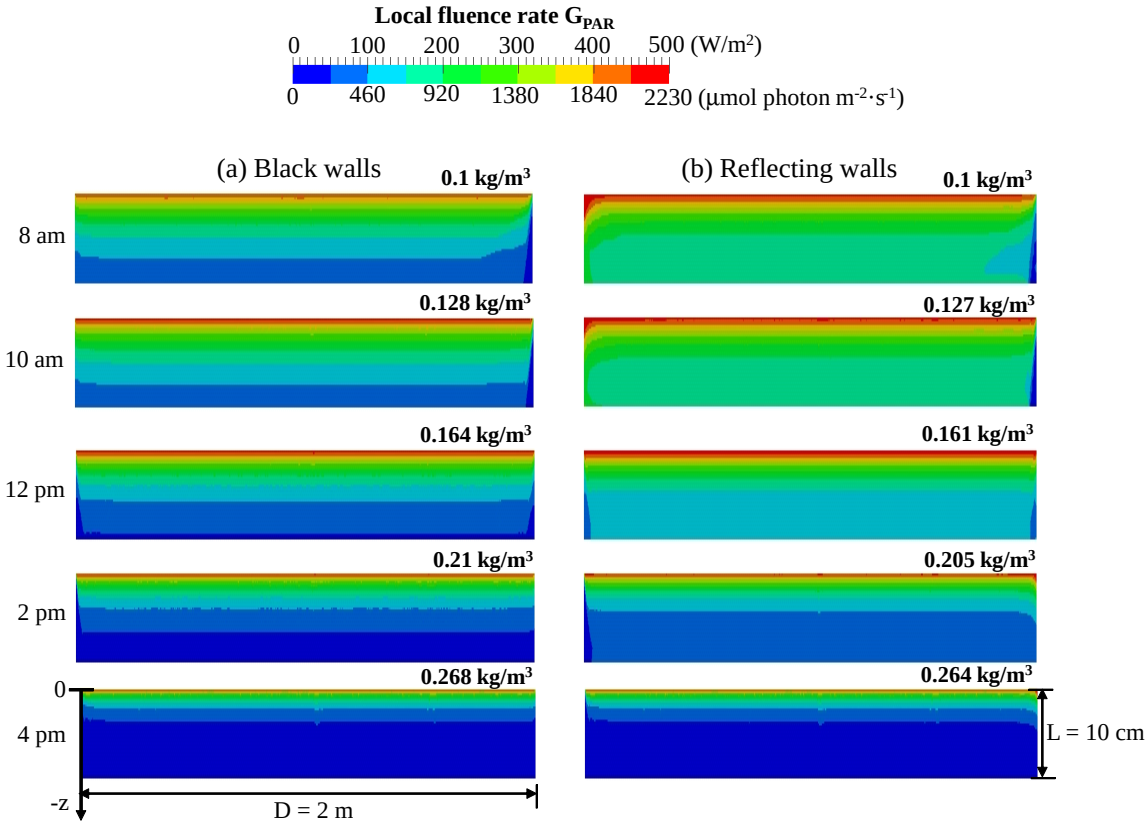

Figure 3: Computed PAR-averaged local fluence rate $G_{PAR}(\mathbf{r})$ on June 21, in Los Angeles at 8:00 am, 10:00 am, 12:00 pm, 2:00 pm, and 4:00 pm in the midplane of an open pond having diameter $D = 2$ m and depth $L = 0.1$ m with (a) black walls or (b) reflecting walls for initial mass concentration $X_0 = 0.1$ kg/m^3.

Figure 4 shows the local PAR-averaged fluence rate $G_{PAR}(\mathbf{r})$ along a vertical cross-section of a 0.1 m thick flat-plate PBR accounting for refraction, at 8:00 am, 10:00 am, 12:00 pm (noon), 2:00 pm, 4:00 pm, and 6:00 pm. Three-dimensional effects were apparent between 10:00 am and 2:00 pm when the sun was near its zenith. During this time, the flat-plate PBR intercepted a small amount of collimated solar radiation. Sunlight was also incident on the PBR vertical windows at glazing angles when reflectance is large. Overall, accounting for refraction reduced slightly the local fluence rate compared with results obtained assuming the PBR wall to be transparent. The relative difference in *C. reinhardtii* mass concentration after 12 h was less than 0.1% when considering or ignoring refraction. Therefore, refraction of sunlight by the front and back windows of the PBR had negligible effects on the mass concentration of microalgae and could be ignored in our simulations.

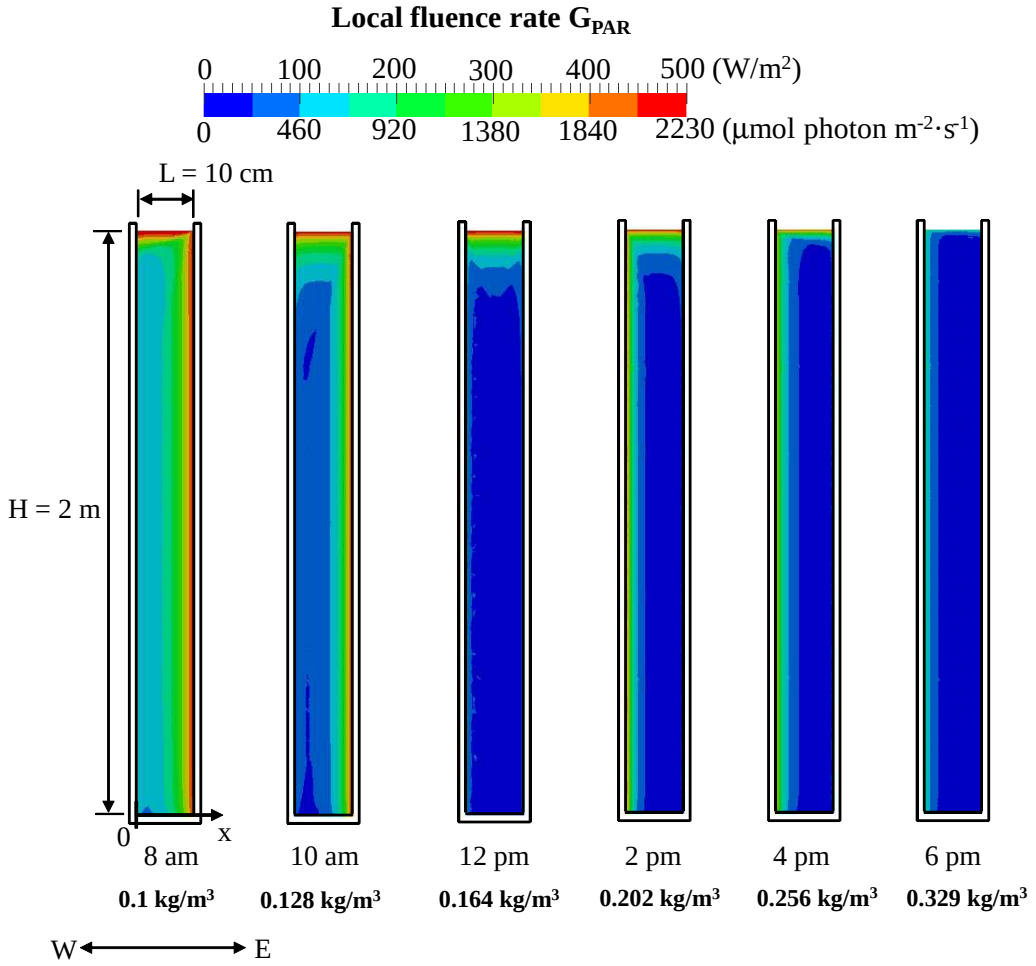

Figure 4: Computed PAR-averaged local fluence rate $G_{PAR}(\mathbf{r})$ on June 21 in Los Angeles at 8:00 am, 10:00 am, 12:00 pm, 2:00 pm, 4:00 pm, and 6:00 pm with refraction by the walls in the midplane of a vertical flat-plate having height $H = 2$ m, width $W = 2$ m, and thickness $L = 0.1$ m with initial mass concentration $X_0 = 0.1$ kg/m^3.

4.3 Tubular photobioreactor

A horizontal tubular photobioreactor oriented in the north-south direction with initial mass concentration $X_0 = 0.1$ kg/m^3 was simulated over 12 hours on June 21. Here, the tubular PBR diameter L was taken as 0.1 m. Figure 5 shows the local PAR-averaged fluence rate $G_{PAR}(\mathbf{r})$ over the cross-section of the pipe at different times of the day. It shows significant multidimensional effects. A darker region developed in the center of the tubular PBR under the combined effects of microalgae growth and the setting of the sun. Given the inherent 2D nature of this type of PBRs, the two-flux approximation could not be used.

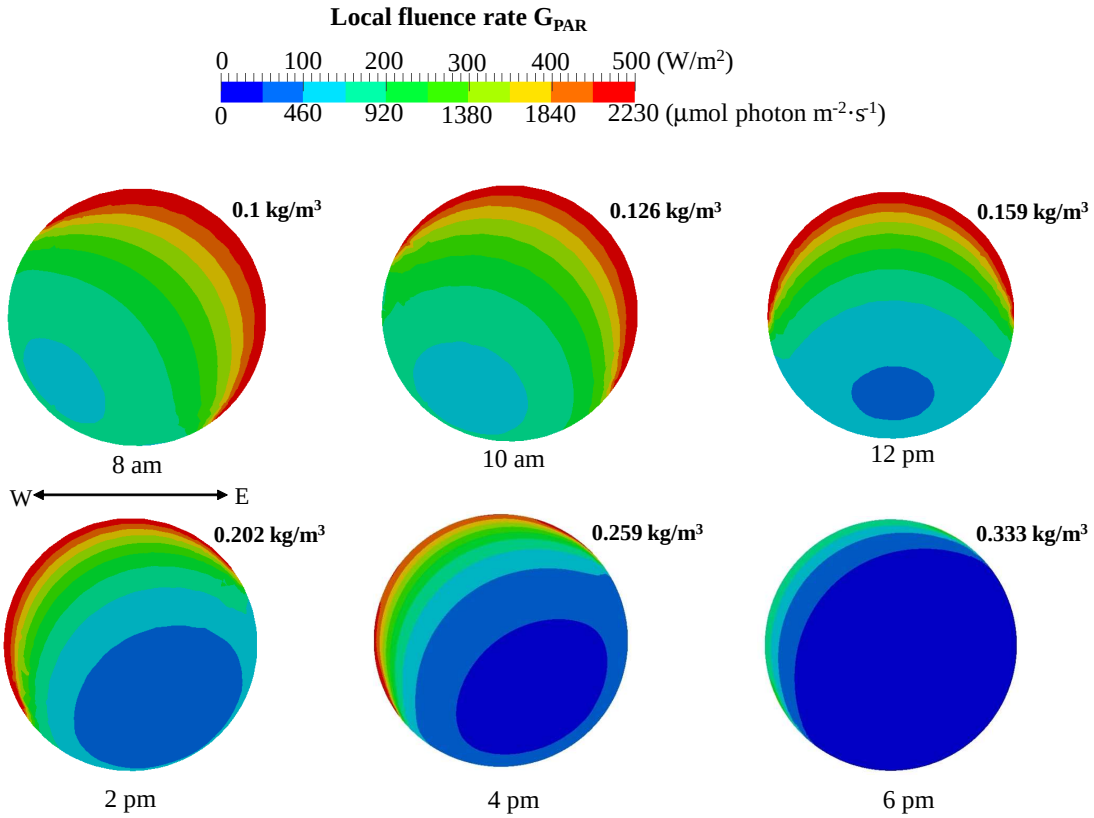

Figure 5: Computed local PAR-averaged fluence rate $G_{PAR}(\mathbf{r})$ on June 21 in Los Angeles at 8:00 am, 10:00 am, 12:00 pm, 2:00 pm, 4:00 pm, and 6:00 pm in the cross-section of north-south oriented tubular PBRs having diameter $L = 0.1$ m with initial mass concentration $X_0 = 0.1$ kg/m^3.

4.4 Two-flux approximation

Figure 6a compares the PAR-averaged local fluence rate $G_{PAR}(z)$ at the centerline of the open pond with black walls at times 8:00 am, 12:00 pm (noon), and 4:00 pm. It also compares the numerical predictions obtained using the DG method with predictions by the two-flux approximation [Equation (22)] and by the simplified two-flux approximation [Equation (23)]. The average relative difference between the numerical predictions using DG method with DOS-ISW and the two-flux approximation for $G_{PAR}(z)$ at the centerline of the open pond ranged between 4 and 10% depending on the time of the day and the location inside the PBR. However, prediction by the two-flux approximation was not able to predict the shadow and other multidimensional effects in the open pond. Moreover, the average total specific growth rate $\bar{\mu}$ predicted based on $G_\lambda(z)$ and $G_{PAR}(z)$ predicted by the two-flux approximation fell within 1 to 7% of its numerically predicted value. These results suggest that the two-flux approximation can be used to determine $G_{PAR}(z)$ and the corresponding $\bar{\mu}$ in open ponds or race ponds with dimensions larger than 2 m when shadow effects become less and less significant. This can be very useful in the design and real time control and operation of open ponds.

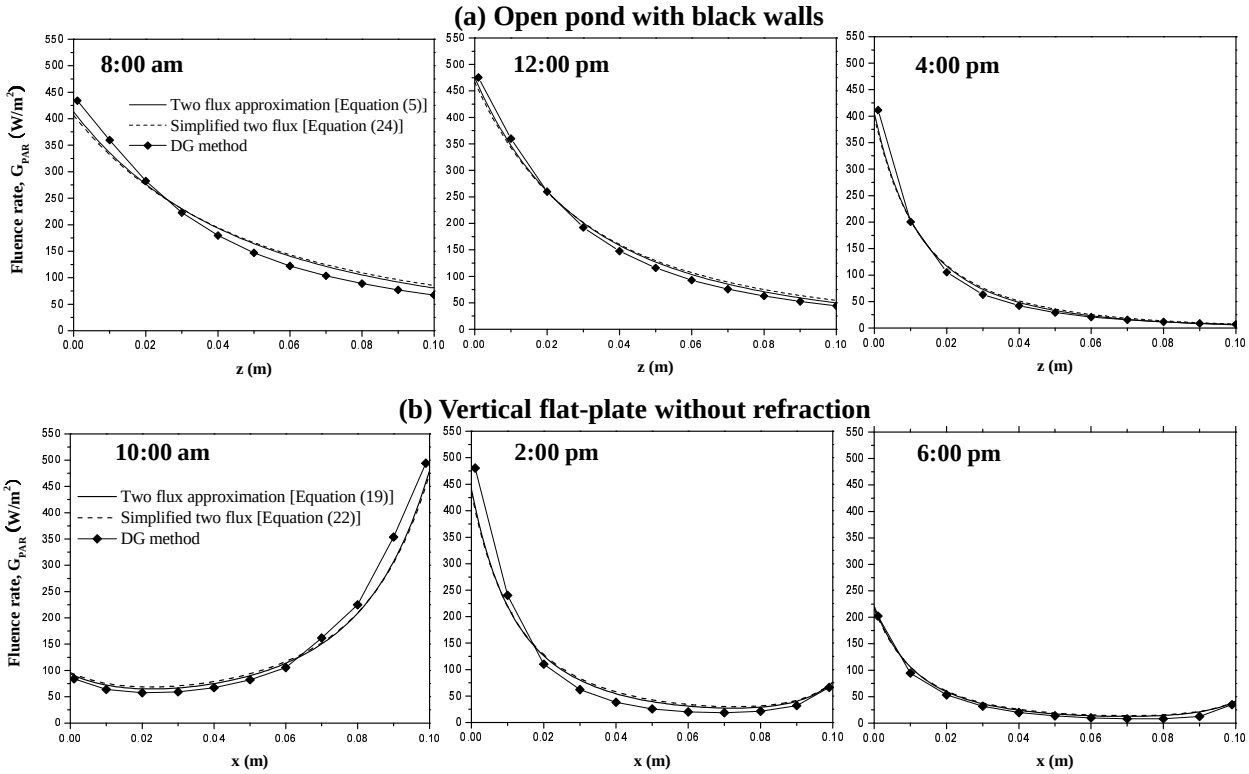

Figure 6: PAR-averaged local fluence rate $G_{PAR}(\mathbf{r})$ predicted on June 21 in Los Angeles at (a) 8:00 am, 12:00 pm, and 4:00 pm in the centerline of an open pond with black walls and (b) at 10:00 am, 2:00 pm, and 6:00 pm across a vertical flat plate PBR by (i) DG method with DOS-ISW, (ii) two-flux approximation [Equations(4)], and (iii) simplified two-flux approximation [Equations(23)]. The open pond featured had diameter $D = 2$ m and depth $L = 0.1$ m while the flat plate PBR had height $H = 2$ m and thickness $L = 0.1$ m. In both cases, the initial mass concentration was $X_0 = 0.1$ kg/m^3.

Figure 6b compares numerical results with predictions from the two-flux approximation [Equation (18)] and the simplified two-flux approximation [Equations (21)]. The maximum relative difference between numerical results and predictions by the two-flux approximation for the local $G_{PAR}(x)$ without refraction ranged between 4 and 22% while the relative differences averaged over the PBR volume were about 2 to 13% depending on the time of the day. The two-flux approximation tended to overpredict $G_{PAR}(x)$ because it was not able to predict the shadow and other multidimensional effects. Moreover, the average total specific growth rate $\bar{\mu}$ estimated using $G_{PAR}(x)$ predicted by the two-flux approximation [Equation (18)] fell within 2 to 10% of its numerically predicted values. Overall, the two-flux approximation predictions of $G_{PAR}(x)$ and the corresponding average total specific growth rate $\bar{\mu}$ in vertical flat-plate PBRs were acceptable. Finally, the average total specific growth rate $\bar{\mu}$ in the vertical flat-plate PBR was found to be larger than that of an open pond of identical depth with black walls at all times except at 12:00 pm because the surface area exposed to sunlight was smaller.

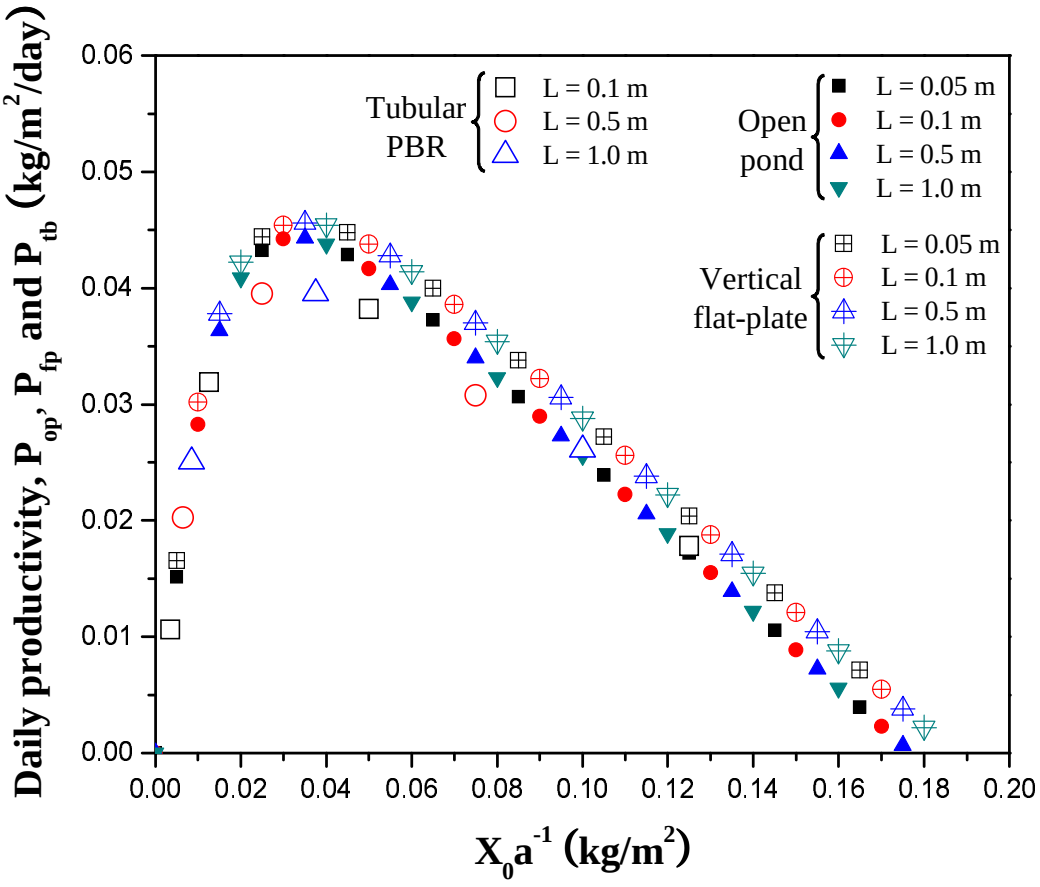

Figure 7: Daily areal biomass productivity per unit illuminated surface area exposed to collimated solar irradiance predicted on June 21 in Los Angeles for open ponds P_{op}, vertical flat-plate PBRs P_{fp}, and tubular PBRs P_{tb} for *C. reinhardtii* as function of X_0a^{-1} with depth or diameter L varying from 0.05 to 1.0 m and initial concentration X_0 between 0.1 and 5.0 kg/m^3. Here, $a_{op} = 1/L$, $a_{fp} = 1/L$, and $a_{tb} = 2/L$.

4.5 Comparison of daily areal biomass productivities

The daily areal biomass productivity of a open pond, expressed in kg/m^2/day, is defined as the mass of microalgae produced after 12 hours of exposure to sunlight per unit illuminated surface area exposed to collimated solar irradiance. It is expressed as

$$P_{op} = \frac{(X_f - X_0)V}{St_f} = \frac{(X_f - X_0)}{Lt_f} \tag{24}$$

where S and V are the illuminated surface area and volume of the PBR while X_f is the final mass concentration and t_f is equal to 1 day. The specific illuminated area of the PBRs, denoted by a (in m^{-1}), is defined as $a = S/V$ [12]. For an open pond of diameter D, thickness L, and illuminated surface area $S = \pi D^2/4$, the specific illuminated area is equal to $a_{op} = 1/L$. In addition, the initial optical thickness of open ponds is expressed as $\beta_\lambda L = (\bar{A}_{abs,\lambda} + \bar{S}_{sca,\lambda})X_0L$ where the average mass cross-sections $\bar{A}_{abs,\lambda}$ and $\bar{S}_{sca,\lambda}$ are

intrinsic properties of the microalgae species. Thus, $X_0 L = X_0 a_{op}^{-1}$ can be considered as representative of the PBR's initial optical thickness.

The daily areal biomass productivity per unit surface area exposed to collimated solar irradiance for vertical flat-plate and tubular PBRs, respectively denoted by P_{fp} and P_{tb} (in kg/m^2/day), are also defined by Equation (24). The specific illuminated area of flat-plate PBRs of thickness L is expressed as $a_{fp} = 1/L$ and that of tubular PBRs of diameter L is equal to $a_{tb} = 2/L$. In other words,

$$P_{fp} = \frac{(X_f - X_0)L}{t_f} \quad \text{and} \quad P_{tb} = \frac{(X_f - X_0)L/2}{t_f} \tag{25}$$

Here also, X_f is the final concentration after a duration t_f of one day.

Figure 7 shows the daily areal biomass productivity of open ponds P_{op}, vertical flat-plate P_{fp}, and tubular PBRs P_{tb} as a function of $X_0 a^{-1}$ for different values of their characteristics length L (i.e., depth, thickness, or diameter) varying from 0.05 to 1.0 m and initial concentration X_0 between 0.0 and 5.0 kg/m^2. The daily areal biomass productivity of vertical flat-plate P_{fp} was calculated based on $\bar{\mu}$ estimated with $G_{PAR}(x)$ predicted by the two-flux approximation, ignoring wall refraction, and accounting for respiration. On the other hand, P_{tb} was calculated numerically based on $G_{PAR}(\mathbf{r})$ and $\bar{\mu}$. It is interesting to note that the daily biomass productivities P_{op}, P_{fp}, and P_{tb} depended uniquely on the product $X_0 a^{-1}$ and not on X_0 and a or L independently.

Moreover, the productivities P_{op}, P_{fp}, and P_{tb} versus $X_0 a^{-1}$ nearly overlapped regardless of the PBR geometry. The maximum daily areal productivity per unit illuminated surface area of these PBRs was P_{max}=0.045 kg/m^2/day for $X_0 a^{-1} = 0.035$ kg/m^2. For $X_0 a^{-1} < 0.035$ kg/m^2, the incident irradiance was not entirely absorbed by microalgae as some photons were absorbed at the bottom of the open pond or transmitted through flat-plate or tubular PBRs. Then, the biomass productivity was low and increased with increasing optical thickness. However, for $X_0^{-1} > 0.035$ kg/m^2, dark region appeared in the PBRs thus decreasing the working illuminated volume while the effects of respiration became significant [50].

Note that the fact that the maximum productivity was identical for PBRs with the same specific illuminated area a irrespective of their geometry has already been predicted by Cornet and Dussap [12] and experimentally validated by Takache *et al.* [16]. Here, we expanded this conclusion by demonstrating that the productivities per unit of illuminated surface area of PBRs are identical (including at their maximum) as long as they feature the same value of optical thickness represented by $X_0 a^{-1}$. These results should be evaluated in combination with the associated capital and operational costs [51]. The same design tool could also be used to investigate shading between cultivation systems but this effort falls outside the scope of the present study.

Finally, the fact that daily biomass productivities P_{op}, P_{fp}, and P_{tb} depend only on the product provides a simple and practical way to design (via a) and to operate (via X_0) these PBRs to achieve maximum productivity in batch mode. Indeed, to achieve the maximum daily production rate from the specific microalgae grown in any of the three PBRs considered, one should geometrically design the PBRs specific illuminated surface area and set the initial concentration X_0 so that $X_0 a^{-1} = 0.035$ kg/m^2. However, one may wonder if these results are valid for (i) other types of PBRs, (ii) for continuous operation, (iii) for different light transfer and growth kinetic models, and if they are supported by experimental evidences.

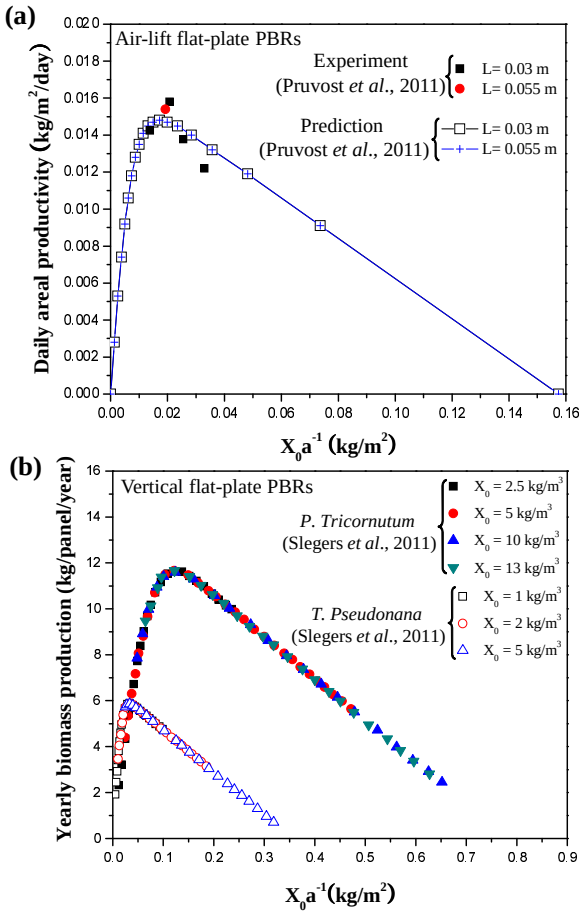

Figure 8: (a) Experimentally measured and predicted daily areal biomass productivity as a function of $X_0 a^{-1}$ [52] for continuous vertical air-lift flat-plate PBR of thickness L equals to 3 or 5.5 cm with *N. oleoabundans*. (b) Collapse of the predicted yearly volumetric biomass productivity shown in Fig. 3 in Ref. [13] plotted as a function of $X_0 a^{-1}$ for 1 m tall vertical flat-plate PBRs in continuous operation with L varying from 0.05 to 0.1 m and X_0 between 1.0 and 13.0 kg/m^3 for *P. tricornutum* and *T. pseudonana*.

4.6 Comparison with experimental data and with other models

Pruvost *et al.* [52] cultivated *Neochloris oleoabundans* in vertical flat-plate air-lift PBRs operated in continuous mode with different thicknesses $L = 0.03$ and 0.055 m. The authors also modeled the process using the two-flux approximation to calculate the fluence rate in the PBRs. The growth kinetics model ignored photoinhibition but accounted for respiration and for the effect of dilution to predict the volumetric and areal productivities. The parameters μ_0, K_S, and μ_s were estimated from experimental data as 0.21 hr^{-1}, 90 μmol photon m$^{-2}\cdot$ s^{-1}, and 0.005 hr^{-1}, respectively. Figure 8a shows the experimentally measured and predicted daily areal biomass productivity of vertical flat-plate air-lift PBRs reported by Pruvost *et al.* [52]. First, it indicates that the productivity measured experimentally had the same order of magnitude as those predicted in this study. Figure 8a also establishes that the areal

productivity of continuous air-lift PBRs was also a unique function of $X_0 a^{-1}$. Note that finding additional experimental data to further validate our results was made difficult by the fact that experimentally the PBR geometry and size as well as the initial concentration are arbitrarily set. Indeed, experimental parametric study similar to that performed numerically in the present study would be very time consuming and potentially costly.

Moreover, Figure 8b shows the simulation results reported by Slegers *et al.* [13] for yearly volumetric biomass production (in kg/m^3/year) for vertical flat-plate PBRs operated in continuous mode with *P. tricornutum* and *T. pseudonana*. Here, the PBR thickness ranged from 0.05 to 0.1 m and concentrations varied between 1.0 and 13.0 kg/m^2. It is very interesting to observe that these data obtained independently using different light and kinetics models collapsed also on a single line when plotted as a function of $X_0 a^{-1}$, whereas they were scattered when plotted as a function of $L = 1/a$ (Figure 3 in the manuscript by Slegers *et al.* [13]). This may be attributed to the fact that the illuminated surface area is closely related to the solar energy input entering the PBR. In other words, the amount of biomass produced remains the same regardless of the PBR geometry for a given amount of solar energy absorbed.

5 CONCLUSION

This study presented accurate 3D numerical simulations for coupled light transfer and growth kinetics in the most commonly used PBRs exposed to collimated and diffuse sunlight in Los Angeles on June 21. The local fluence rate was predicted on a spectral basis by solving the 3D RTE. The temporal evolution of microalgae mass concentration was predicted by accounting for light saturation, photolimitation, and respiration. In open ponds, the reflecting walls resulted in a more uniform light distribution and increased the local fluence rate. However, the difference in overall biomass concentration after 12 hours was negligible. Similarly, refraction by the container walls, in vertical flat-plate PBRs, had no significant effect on the microalgae concentration. The study demonstrated that the two-flux approximation can be used to estimate the local fluence rate in open (or race) ponds and flat-plate PBRs for all practical purposes including designing, controlling, and operating PBRs. Finally, the daily areal biomass productivity per unit footprint was found to depend uniquely on the initial optical thickness represented by $X_0 a^{-1}$ for open ponds and tubular PBRs operated in batch mode. Similar results were obtained for the daily productivity per unit surface area illuminated for flat-plate PBRs. What's more, the same conclusions were drawn be revisiting both experimental data and numerical simulations reported in the literature for similar and other PBR types cultivating other microorganisms in continuous mode. The parameter $X_0 a^{-1}$ is useful and simple for designing (via a) and operating (via X_0) these PBRs at their maximum productivity.

References

[1] L. Pilon, H. Berberoğlu, and R. Kandilian, "Radiation transfer in photobiological carbon dioxide fixation and fuel production by microalgae", *Journal of Quantitative Spectroscopy and Radiative Transfer*, vol. 112, no. 17, pp. 2639 – 2660, 2011.

[2] K. Skjånes, P. Lindblad, and J. Muller, "BioCO$_2$ - a multidisciplinary, biological approach using solar energy to capture CO$_2$ while producing H$_2$ and high value products", *Biomolecular Engineering*, vol. 24, no. 4, pp. 405–413, 2007.

[3] J.H. Yoon, S.J. Sim, M.S. Kim, and T.H. Park, "High cell density culture of *Anabaena variabilis* using repeated injections of carbon dioxide for the production of hydrogen", *International Journal of Hydrogen Energy*, vol. 27, no. 11-12, pp. 1265–1270, 2002.

[4] J.A. Asenjo and J.C. Merchuk, *Bioreactor System Design*, Marcel Dekker, New York, NY, 1995.

[5] L. Barsanti and P. Gualtieri, *Algae: Anatomy, Biochemistry, and Biotechnology*, CRC Press, Boca Raton, FL, 2005.

[6] M. Morweiser, O. Kruse, B. Hankamer, and C. Posten, "Developments and perspectives of photobioreactors for biofuel production", *Applied Microbiology and Biotechnology*, vol. 87, pp. 1291–1301, 2010.

[7] C.U. Ugwu, H. Aoyagi, and H. Uchiyama, "Photobioreactors for mass cultivation of algae", *Bioresource Technology*, vol. 99, pp. 4021 – 4028, 2008.

[8] C. Posten, "Design principles of photo-bioreactors for cultivation of microalgae", *Engineering in Life Sciences*, vol. 9, pp. 165–177, 2009.

[9] S. Aiba, "Growth kinetics of photosynthetic microorganisms", *Advances in Biochemical Engineering/Biotechnology*, vol. 23, pp. 85–156, 1982.

[10] J.-F. Cornet, C.G. Dussap, and G. Dubertret, "A structured model for simulation of cultures of the cyanobacterium *Spirulina platensis* in photobioreactors: I. Coupling between light transfer and growth kinetics", *Biotechnology and Bioengineering*, vol. 40, no. 7, pp. 817–825, 1992.

[11] L. Pottier, J. Pruvost, J. Deremetz, J.-F. Cornet, J. Legrand, and C.G. Dussap, "A fully predictive model for one-dimensional light attenuation by C*hlamydomonas reinhardtii* in a torous photobioreactor", *Biotechnology and Bioengineering*, vol. 91, pp. 569–582, 2005.

[12] J.F. Cornet and C.G. Dussap, "A simple and reliable formula for assessment of maximum volumetric productivities in photobioreactors", *Biotechnology Progress*, vol. 25, pp. 424–435, 2009.

[13] P.M. Slegers, R.H. Wijffels, G. van Straten, and A.J.B. van Boxtel, "Design scenarios for flat panel photobioreactors", *Applied Energy*, vol. 88, pp. 3342 – 3353, 2011.

[14] J.-F. Cornet, C.G. Dussap, P. Cluzel, and G. Dubertret, "A structured model for simulation of cultures of the cyanobacterium *Spirulina platensis* in photobioreactors: II. Identification of kinetic parameters under light and mineral limitations", *Biotechnology and Bioengineering*, vol. 40, no. 7, pp. 826–834, 1992.

[15] J.-F. Cornet, C.G. Dussap, J.B. Gross, C. Binois, and C. Lasseur, "A simplified monodimensional approach for modeling coupling between radiant light transfer and growth kinetics in photobioreactors", *Chemical Engineering Science*, vol. 50, no. 9, pp. 1489–1500, 1995.

[16] H. Takache, G. Christophe, J.-F. Cornet, and J. Pruvost, "Experimental and theoretical assessment of maximum productivities for the microalgae chlamydomonas reinhardtii in two different geometries of photobioreactors", *Biotechnology Progress*, vol. 26, pp. 431–440, 2010.

[17] H. Berberoğlu, A. Melis, and L. Pilon, "Radiation characteristics of *Chlamydomonas reinhardtii* CC125 and its truncated chlorophyll antenna transformants *tla1*, *tlaX*, and *tla1-CW*$^+$", *International Journal of Hydrogen Energy*, vol. 33, no. 22, pp. 6467–6483, 2008.

[18] M.F. Modest, *Radiative Heat Transfer*, Academic Press, San Diego, CA, 2003.

[19] H. Berberoğlu, J. Yin, and L. Pilon, "Light transfer in bubble sparged photobioreactors for H_2 production and CO_2 mitigation", *International Journal of Hydrogen Energy*, vol. 32, pp. 2273 – 2285, 2007.

[20] J.F. Cornet and J. Albiol, "Modeling photoheterotrophic growth kinetics of *Rhodospirillum rubrum* in rectangular photobioreactors", *Biotechnology Progress*, vol. 16, pp. 199–207, 2000.

[21] S. Fouchard, J. Pruvost, B. Degrenne, M. Titica, and J. Legrand, "Kinetic modeling of light limitation and sulfur deprivation effects in the induction of hydrogen production with *Chlamydomonas reinhardtii*: Part I. model development and parameter identification", *Biotechnology and Bioengineering*, vol. 102, no. 1, pp. 232–245, 2009.

[22] Z.C. Wheaton and G. Krishnamoorthy, "Modeling radiative transfer in photobioreactors for algal growth", *Computers and Electronics in Agriculture*, vol. 87, pp. 64 – 73, 2012.

[23] H. Berberoğlu, J. Yin, and L. Pilon, "Simulating light transfer in a bubble sparged photobioreactor for simultaneous hydrogen fuel production and CO_2 mitigation", *International Journal of Hydrogen Energy*, vol. 32, no. 13, pp. 2273–2285, 2007.

[24] T.E. Murphy and H. Berberoğlu, "Effect of algae pigmentation on photobioreactor productivity and scale-up: A light transfer perspective", *Journal of Quantitative Spectroscopy and Radiative Transfer*, vol. 112, pp. 2826 – 2834, 2011.

[25] R.J. Geider, H.L. MacIntyre, and T.M. Kana, "A dynamic model of photoadaptation in phytoplankton", *Limnology and Oceanography*, vol. 41, pp. 1–15, 1996.

[26] Q. Huang, L. Yao, T. Liu, and J. Yang, "Simulation of the light evolution in an annular photobioreactor for the cultivation of *Porphyridium cruentum*", *Chemical Engineering Science*, vol. 84, pp. 718 – 726, 2012.

[27] A. Muller-Feuga, R. Le Guédes, and J. Pruvost, "Benefits and limitations of modeling for optimization of *Porphyridium cruentum* cultures in an annular photobioreactor", *Journal of Biotechnology*, vol. 103, pp. 153 – 163, 2003.

[28] J. Pruvost, J. F. Cornet, V. Goetz, and J. Legrand, "Theoretical investigation of biomass productivities achievable in solar rectangular photobioreactors for the cyanobacterium arthrospira platensis", *Biotechnology Progress*, vol. 28, pp. 699–714, 2012.

[29] J. Pruvost, J. Legrand, P. Legentilhomme, and A. Muller-Feuga, "Simulation of microalgae growth in limiting light conditions: Flow effect", *AIChE Journal*, vol. 48, no. 5, pp. 1109–1120, 2002.

[30] F.G. Acién Fernández, F. García Camacho, J.A. Sánchez Pérez, J.M. Fernández Sevilla, and E. Molina Grima, "A model for light distribution and average solar irradiance inside outdoor tubular photobioreactors for the microalgal mass culture", *Biotechnology and Bioengineering*, vol. 55, no. 5, pp. 701–714, 1997.

[31] J. Dauchet, S. Blanco, J.-F. Cornet, M. El Hafi, V. Eymet, and R. Fournier, "The practice of recent radiative transfer Monte Carlo advances and its contribution to the field of microorganisms cultivation in photobioreactors", *Journal of Quantitative Spectroscopy and Radiative Transfer*, , no. 0, pp. –, 2012.

[32] W.H. Reed and T.R. Hill, "Triangular mesh method for the neutron transport equation", Tech. Rep. LA-UR-73-479, Los Alamos Scientific Laboratory Report, Los Alamos, NM, 1973.

[33] X. Cui and B.Q. Li, "A discontinuous finite-element formulation for multidimensional radiative transfer in absorbing, emitting, and scattering media", *Numerical Heat Transfer Part B-Fundamentals*, vol. 46, no. 5, pp. 399–428, 2004.

[34] X. Cui and B.Q. Li, "Discontinuous finite element solution of 2-D radiative transfer with and without axisymmetry", *Journal of Quantitative Spectroscopy and Radiative Transfer*, vol. 96, no. 3-4, pp. 383–407, 2005.

[35] X. He, E. Lee, L. Wilcox, R. Munipalli, and L. Pilon, "A high-order accurate GPU-based radiative transfer equation solver for combustion and propulsion applications", *Numerical Heat Transfer Part B-fundamentals*, 2012 (accepted).

[36] J.S. Hesthaven and L. Koblinger, *Nodal Discontinuous Galerkin Methods: Algorithms, Analysis, and Applications*, Springer, New York, NY, 2007.

[37] J.M. Zhao and L.H. Liu, "Discontinuous spectral element method for solving radiative heat transfer in multidimensional semitransparent media", *Journal of Quantitative Spectroscopy and Radiative Transfer*, vol. 107, no. 1, pp. 1–16, 2007.

[38] I.J. Dunn, E. Heinzle, J. Ingham, and J.E. Prenosil, *Biological Reaction Engineering: Dynamic Modelling Fundamentals with Simulation Examples*, Wiley-VCH, 2^{nd} edition, 2003.

[39] K. J. Versyck, J. E. Claes, and J. F. Van Impe, "Practical identification of unstructured growth kinetics by application of optimal experimental design", *Biotechnology Progress*, vol. 13, no. 5, pp. 524–531, 1997.

[40] H. Berberoğlu and L. Pilon, "Maximizing solar to H_2 energy conversion efficiency of outdoor photobioreactors using mixed cultures", *International Journal of Hydrogen Energy*, vol. 35, pp. 500–510, 2010.

[41] G.M. Hale and M.R. Querry, "Optical constants of water in the 200-nm to 200-μm wavelength region", *Applied Optics*, vol. 12, pp. 555–563, 1973.

[42] H. Berberoğlu and L. Pilon, "Experimental measurement of the radiation characteristics of *Anabaena variabilis* ATCC 29413-U and *Rhodobacter sphaeroides* ATCC 49419", *International Journal of Hydrogen Energy*, vol. 32, no. 18, pp. 4772–4785, 2007.

[43] E. Lee, R.-L. Heng, and L. Pilon, "Spectral optical properties of selected photosynthetic microalgae producing biofuels", *Journal of Quantitative Spectroscopy and Radiative Transfer*, vol. 114, pp. 122 – 135, 2013.

[44] C. Gueymard, "SMARTS Code, Version 2.9.2 User's direct beam spectral irradiance data for photovoltaic cell Manual", Solar Consulting Services, http://rredc.nrel.gov/solar/models/SMARTS, 2002.

[45] W.A. Fiveland and R.A. Wessel, "Numerical model for predicting performance of three-dimensional pulverized-fuel fired furnaces", *ASME Journal of Engineering for Gas Turbines and Power*, vol. 110, no. 1, pp. 117–126, 1988.

[46] E.H. Chui and G.D. Raithby, "Computation of radiant-heat transfer on a nonorthogonal mesh using the finite-volume method", *Numerical Heat Transfer Part B-Fundamentals*, vol. 23, no. 3, pp. 269–288, 1993.

[47] H.-S. Li, G. Flamant, and J.-D. Lu, "A new discrete ordinate algorithm for computing radiative transfer in one-dimensional atmospheres", *Journal of Quantitative Spectroscopy and Radiative Transfer*, vol. 83, pp. 407–421, 2004.

[48] M. Janssen, L. De Bresser, T. Baijens, J. Tramper, L.R. Mur, J.F.H. Snel, and R.H. Wijffels, "Scale-up aspects of photobioreactors: effects of mixing-induced light/dark cycles", *Journal of Applied Phycology*, vol. 12, pp. 225–237, 2000.

[49] A. Morel and R.C. Smith, "Relation between total quanta and total energy for aquatic photosynthesis", *Limnology and Oceanography*, vol. 19, pp. 591–600, 1974.

[50] H. Takache, J. Pruvost, and J.-F. Cornet, "Kinetic modeling of the photosynthetic growth of *Chlamydomonas reinhardtii* in a photobioreactor", *Biotechnology Progress*, vol. 28, no. 3, pp. 681–692, 2012.

[51] D. Chaumont, "Biotechnology of algal biomass production: a review of systems for outdoor mass culture", *Journal of Applied Phycology*, vol. 5, pp. 593–604, 1993.

[52] J. Pruvost, G. Van Vooren, B. Le Gouic, A. Couzinet-Mossion, and J. Legrand, "Systematic investigation of biomass and lipid productivity by microalgae in photobioreactors for biodiesel application", *Bioresource Technology*, vol. 102, pp. 150 – 158, 2011.

[53] A. Richmond, "Efficient utilization of high irradiance for production of photoautotropic cell mass: a survey", *Journal of Applied Phycology*, vol. 8, pp. 4 – 5, 1996.

[54] A. Richmond, H. Qiang, "Principles for efficient utilization of light for mass production of photoautotrophic microorganisms", *Applied Biochemistry and Biotechnology*, vol. 63 – 65, pp. 649 – 658, 1997.

[55] A. Richmond, "Principles for attaining maximal microalgal productivity in photobioreactors: an overview", *Hydrobiology*, vol. 512, pp. 33 – 37, 2004.

[56] F. Le Borgne, J. Pruvost, "Investigation and modeling of biomass decay rate in the dark and its potential influence on net productivity of solar photobioreactors for microalga Chlamydomonas reinhardtii and cyanobacterium Arthrospira platensis", *Bioresource Technology*, vol. 138, pp. 271 – 276, 2013.